

# Group Secret-Key Generation using Algebraic Rings in Three-User Wireless Networks

Manish Rao and J. Harshan

## Abstract

Physical-layer Group Secret-Key (GSK) generation is an effective way of synthesizing symmetric keys across multiple nodes in wireless networks. Unlike the case of two-user key generation, GSK generation necessitates some nodes to act as *facilitators*, which broadcast linear combinations of the channel realizations thereby assisting all the nodes to witness the intended common source of randomness. However, in practice, radio devices are designed to transmit symbols from finite complex constellations, and as a result, the channel realizations are typically quantized by the facilitator which in turn impacts the overall secret-key rate. Identifying this issue, we propose a class of GSK generation protocols, called Symmetrically Quantized GSK (SQGSK) protocols, in a network of three nodes. In the proposed protocols, due to quantization of symbols at the facilitator, the other two nodes also quantize their channel realizations, and use them appropriately to generate the keys. Under special conditions, we analytically show that the SQGSK protocols provide higher key-rate than the baselines wherein only the facilitator quantizes the channel realizations. We use extensive simulations to demonstrate the benefits of the proposed protocols when the facilitator employs finite constellations such as 4-, 16-, and 64-QAM.

## Index Terms

Physical-layer key generation, common source of randomness, security, wireless networks

## I. INTRODUCTION

Physical-layer key generation is an effective way of synthesizing symmetric keys for securing communication between wireless nodes. In the simplest model of two-node key generation, radio devices witness correlated source of randomness by observing the temporal variation of the wireless channel between them. A popular way to implement such an idea is to exchange pilot symbols (in time-division duplex manner) within the coherence-interval thereby exploiting the channel reciprocity property [1]. This line

Manish Rao and J. Harshan are with the Department of Electrical Engineering, Indian Institute of Technology Delhi, India. Email: manish.eee15@ee.iitd.ac.in, jharshan@ee.iitd.ac.in. Part of this work will appear in the proceedings of International Conference on Signal Processing and Communications 2018 [25].

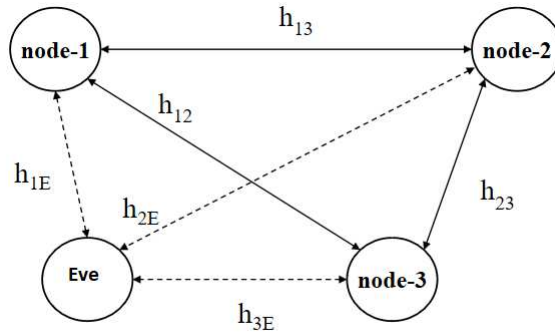


Fig. 1. Network model of interest with three interconnected wireless nodes, which intend to generate a group secret key in the presence of a passive eavesdropper. We assume pair-wise reciprocity in our model, i.e.,  $h_{jk} = h_{kj}$  for  $k, j, \in \{1, 2, 3, E\}$  such that  $k \neq j$ . All the channels in the above model are assumed to be statistically independent.

of key generation has been well studied with various applications such as radio-frequency communication and optical communication.

A generalization of two-node physical-layer key generation is group secret-key (GSK) generation [20]-[21], wherein more than two nodes in the network generate a shared secret-key by observing an appropriately chosen common source of randomness (CSR). One of the main questions in such a scenario is “*What is the CSR that the nodes should witness?*” To illustrate, in the case of the three-node network shown in Fig. 1, the total set of available channels is  $\{h_{12}, h_{13}, h_{23}\}$ , where  $h_{jk}$  denotes the complex baseband wireless channel between node- $j$  and node- $k$ . With this setup, the CSR can be any *non-empty* subset of the available channels. Irrespective of the choice of the CSR, observe that some nodes in the network have to learn the channel realizations of the adjacent pairs, and this cannot be achieved by exchanging pilot symbols among them. For instance, if the CSR is  $h_{12}$ , then node-3 cannot learn this channel during the pilot transmission phase, and therefore either node-1 or node-2 (or both) has (have) to help node-3 in learning  $h_{12}$ . In general, an inherent property of physical-layer GSK generation is that some channel realizations can be directly obtained using pilots, while some of them have to be shared by special nodes, called *facilitators*. This implies that the facilitators need to transmit Gaussian distributed complex numbers with infinite precision. However, in practice, radio devices are designed to transmit baseband symbols from finite constellations. As a result, quantized versions of the channel realizations have to be transmitted by the facilitators, and this leads to disparity in the noise levels of the CSR observed at various nodes in the network. In this paper, we address this disparity and discuss new methods to generate GSK by acknowledging the fact that the CSR at some nodes are more corrupted than at others.

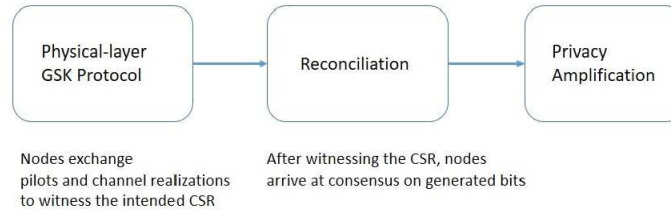


Fig. 2. This work addresses practical physical-layer GSK protocols (captured by the first block in the above block-diagram) to assist the nodes in Fig. 1 to witness the intended CSR. We use the level-crossing algorithm in [1] for the reconciliation process. We omit the privacy amplification block as it is out of scope of this work.

### A. Contributions

The main contributions of this work are listed below:

- We address physical-layer GSK generation among three nodes in a wireless network as shown in Fig. 1. Particularly, we are interested in developing a practical GSK method (the first block in Fig. 2), wherein the nodes have the constraint of transmitting baseband symbols from finite complex constellations. We highlight that this practical aspect of GSK generation has not been studied in the literature. In our framework of practical GSK generation, the facilitators are restricted to quantize the channel realizations directly to points in complex constellations such as quadrature amplitude modulation (QAM). GSK protocols wherein only the facilitators quantize the complex channel realizations are considered as baselines to evaluate the contributions of this work, and those baselines are referred to as Asymmetrically Quantized GSK (AQGSK) protocols. (See Section II and Section III).
- To address the constraints imposed on the facilitator, we propose a practical GSK protocol, referred to as Symmetrically Quantized GSK (SQGSK), wherein due to the quantization of symbols at the facilitator, the other two nodes also quantize their channel realizations, and use them appropriately to generate keys. This *forced-quantization* at the other two nodes, although not necessary, will make sure that the three nodes have common source of randomness with high correlation. We first give an intuitive explanation on the benefits of SQGSK, and then information-theoretically prove its advantages over the baseline under special conditions (See Section IV-C). Through simulations, we show that SQGSK outperforms the baseline with at most 43%, 9% and 4% increase in key-rate, when the facilitator employs 4-, 16- and 64-QAM to quantize the channel realizations, respectively (See Section VI).
- To study the leakage aspects of the GSK protocol, we consider a passive eavesdropper model as shown in Fig. 1, wherein the eavesdropper (represented as Eve) can perfectly recover the symbols

transmitted by each of the legitimate nodes. However, by the virtue of her geographical location, the eavesdropper cannot learn the channels  $\{h_{12}, h_{13}, h_{23}\}$  using the pilot symbols transmitted by the legitimate nodes. We present leakage analysis of the CSR in the SQGSK protocol, and theoretically prove that the residual entropy at an external eavesdropper is strictly less than the entropy of the CSR (See Section IV-D). We show that SQGSK leaks 25% to 50% of the CSR depending on the size of the constellation. To circumvent this limitation of the SQGSK protocol, we propose another practical key generation protocol, referred to as the Algebraic SQGSK protocol (See Section V), wherein the facilitator transmits a linear combination of the quantized versions of the channel realizations over a suitable algebraic ring. Subsequently, we show that this algebraic result can be used by the other nodes to witness a noisy version of the common source of randomness. Under special conditions, we theoretically prove that the key-rate offered by the Algebraic SQGSK protocol is higher than the baseline (See Section V-C), and also prove that the Algebraic SQGSK protocol incurs zero leakage of the CSR to an external eavesdropper (See Section V-D). Through simulations, we show that Algebraic SQGSK outperforms the baseline with at most 230%, 57% and 24% increase in key-rate, when the facilitator employs 4-, 16- and 64-QAM to quantize the channel realizations, respectively (See Section VI).

- In the last part of this work, we propose a multi-level quantization algorithm in order to capitalize on the discrete nature of the CSR in the SQGSK protocols. In this part, our contribution is in the second block of the block-diagram in Fig. 2. Through simulations, we show that the multi-level quantization idea provides significant benefits in key-rates (74% with 16-QAM and 34% with 64-QAM) at high signal-to-noise ratio (SNR) values when used in conjunction with the Algebraic SQGSK protocol. (See Section VII)

## B. Our Approach

When proposing practical protocols to synthesize GSKs, we analyze their key-rate by applying information-theoretical results in no additive-noise scenario so as to capture the effect of quantization noise. For instance, with reference to Fig. 1, if the channel realization  $h_{12}$  is chosen as the CSR, then node-1 and node-2 observe  $r_1 = h_{12}$  and  $r_2 = h_{12}$ , respectively (due to channel reciprocity), whereas node-3 observes  $r_3 = h_{12} + z_3$  such that  $z_3$  captures the quantization noise introduced by the facilitator. In such a scenario, the key-rate is information-theoretically determined by [12]

$$\frac{1}{N} \min(I(r_1; r_2), I(r_1; r_3), I(r_2; r_3)) = \frac{1}{N} \min(H(h_{12}), I(h_{12}; h_{12} + z_3)). \quad (1)$$

where  $H(\cdot)$  denotes the differential-entropy operator,  $I(\cdot; \cdot)$  denotes the mutual information operator, and  $N$  denotes the number of channel-uses needed so that the three nodes witness the CSR. To analytically

substantiate the superiority of one GSK protocol over the other, we compare the mutual information expressions in (1) in no additive-noise scenario, and supplement those results through extensive simulations in the presence of additive noise. To showcase the effectiveness of the proposed protocols, we use them in conjunction with the well known level-crossing algorithm [1], which is mainly used for reconciliation on the generated secret bits. Due to space constraints, we omit a detailed description of the level-crossing algorithm and refer to the readers to [1] for more details.

### C. Related Work

Physical-layer key generation between two radio devices is well studied starting from theory, that focus on fundamental limits [2], to test bed developments that showcase proof of concepts [3]. A wide range of contributions exist in this topic, wherein the specific choice of common source of randomness [4], [5], [6], [7], [8], used to generate the keys depend on wireless platforms such as OFDM [9], multiple-input multiple-output (MIMO) systems [10], and fibre optical networks [11], to name a few. Extending the idea of key generation between two radio devices, some contributions have also studied models involving third-party relay(s) to help generate secret-keys between nodes that are out of radio-frequency range. Within this class, [13],[14] have focused on protocols for exchanging messages so as to (i) reduce the latency, and (ii) to secure the generated keys from an external eavesdropper, while some have considered *honest-but-curious* relays that help in the key generation process, but also are curious to listen to the messages [15]. The latter framework focuses on designing protocols to generate keys via untrusted relays, and yet minimize leakage of information to them [16], [17]. A generalization of relay-assisted secret-key generation is the concept of wireless physical-layer group secret-key (GSK) generation, wherein a group of nodes in a network generate a shared secret-key by observing a common source of randomness. For GSK generation using pair-wise channels, we refer the readers to [18], [20], for key generation using received signal strength indicator (RSSI) values, we refer the readers to [19], [21], for group keys using channel estimates, we refer to [22]. Although there is rich literature on physical-layer GSK generation using RSSI values and channel estimates, questions on practicality of such approaches are missing. One such practical aspect is the involvement of facilitators, which need to transmit quantized versions of the channel realizations to other nodes in the network.

Notations: We use  $x \sim \mathcal{CN}(0, \sigma^2)$  to represent a circularly symmetric complex Gaussian random variable with mean 0 variance  $\sigma^2$ . The set of all integers and Gaussian integers are denoted by  $\mathbb{Z}$  and  $\mathbb{Z}[i]$ , respectively, where  $i = \sqrt{-1}$ . The set  $\mathbb{Z}_p$ , for some integer  $p > 1$ , is given by  $\{0, 1, 2, \dots, p-1\}$ . The mutual information between two random variables  $x$  and  $y$  is denoted by  $I(x; y)$ , and  $H(x)$  denotes the (differential) entropy of a (continuous) random variable  $x$ . The probability mass function (PMF) on

a discrete random variable  $x$  is denoted by  $P(x)$ . Assuming that the realizations of a discrete random variable  $x$  are ordered, we use  $x_j$  to denote the  $j$ -th realization. Furthermore, the probability that a discrete random variable  $x$  takes the value  $x_j$  is denoted by  $\text{Prob}(x = x_j)$ . We denote the set of all complex numbers by  $\mathbb{C}$ . Given two sets  $\mathcal{S}_1 \subset \mathbb{C}$  and  $\mathcal{S}_2 \subset \mathbb{C}$ , the direct sum  $\mathcal{S}_1 \oplus \mathcal{S}_2$  is given by  $\{s_1 + s_2 \mid s_1 \in \mathcal{S}_1, s_2 \in \mathcal{S}_2\}$ . The acronym AWGN refers to additive white Gaussian noise. The number of elements in the set  $\mathcal{S}$  is denoted by  $|\mathcal{S}|$ .

## II. GROUP SECRET KEY GENERATION

We consider a wireless network comprising three nodes, denoted by node-1, node-2 and node-3 as shown in Fig. 1. In this network model, the channel between any two nodes is assumed to be frequency-flat and remain quasi-static for a block of four channel-uses. The wireless channel between node- $j$  and node- $k$ , for  $j \neq k$  is represented by a complex Gaussian random variable  $h_{jk} \sim \mathcal{CN}(0, 1)$ . We assume that the channels  $\{h_{12}, h_{13}, h_{23}\}$  are statistically independent and exhibit pair-wise reciprocity within the coherence-block, i.e.,  $h_{jk} = h_{kj}$  for  $j \neq k$ . We also assume that all the nodes witness AWGN distributed as  $\mathcal{CN}(0, \sigma^2)$ . The three nodes intend to generate a GSK by observing a subset of the channel realizations  $\{h_{12}, h_{13}, h_{23}\}$ . This subset is referred to as the CSR in our model. To learn the CSR, the three nodes broadcast the pilot symbols turn-by-turn within each coherence-block, using which the receiving nodes learn the corresponding channel realizations. Subsequently, one of the nodes, referred to as the facilitator, broadcasts a combination of its observed channel realizations to assist all the nodes in learning the CSR. Consolidating the CSR observed over several coherence-blocks, the three nodes then apply a suitable key generation algorithm to synthesize a GSK. We denote the channel realizations based on the coherence-block index  $l$  for  $l = 1, 2, \dots, L$ , i.e.,  $\mathcal{H}(l) = \{h_{12}(l), h_{13}(l), h_{23}(l)\}$ . Note that the facilitator must transmit the channel realizations in such a way to prevent leakage to an external eavesdropper. In the next section, we present one such GSK protocol wherein the three nodes have to witness the CSR  $\{h_{12}(l), h_{13}(l)\}$ , for  $1 \leq l \leq L$ .<sup>1</sup>

### A. GSK protocol

We present a detailed description of the GSK protocol [23] as depicted in Fig. 3. Specifically, for a given coherence-block  $l \in \{1, 2, \dots, L\}$ , the protocol comprises of four phases, i.e.,  $N = 4$ :

<sup>1</sup>It is straightforward to extend the considered GSK protocol to assist the users in witnessing  $\{h_{12}(l), h_{13}(l), h_{23}(l)\}$  as the CSR. Since we are interested in studying the quantization effects on the CSR, our choice of  $\{h_{12}(l), h_{13}(l)\}$  as the CSR serves the purpose.

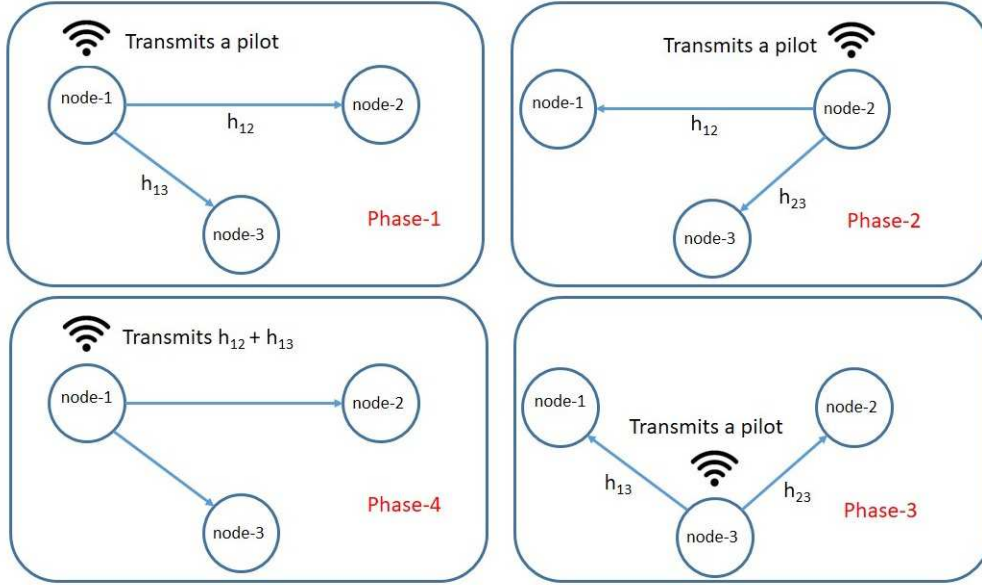


Fig. 3. A four-phase GSK protocol depicting exchange of pilot symbols and channel realizations among the three nodes. Using the above protocol, the three nodes arrive at the common source of randomness  $\{h_{12}, h_{13}\}$ , using which secret keys are synthesized. In this protocol, node-1 acts as the facilitator to help node-2 and node-3 in learning  $h_{13}(l)$  and  $h_{12}(l)$ , respectively.

**Phase 1:** node-1 transmits a pilot symbol  $x = 1$ , which is used by node-2 and node-3 to estimate the channels  $h_{12}(l)$  and  $h_{13}(l)$ , respectively, as

$$\theta_2^{(1)}(l) = h_{12}(l) + e_2^{(1)}(l) \text{ and } \theta_3^{(1)}(l) = h_{13}(l) + e_3^{(1)}(l), \quad (2)$$

where  $e_2^{(1)}(l) \sim \mathcal{CN}(0, \gamma)$  and  $e_3^{(1)}(l) \sim \mathcal{CN}(0, \gamma)$  denote the channel estimation errors at node-2 and node-3, respectively. The superscripts denote the phase number in each coherence-block.

**Phase 2:** node-2 transmits a pilot symbol  $x = 1$ , which is used by node-1 and node-3 to estimate the channels  $h_{12}(l)$  and  $h_{23}(l)$ , respectively, as

$$\theta_1^{(2)}(l) = h_{12}(l) + e_1^{(2)}(l) \text{ and } \theta_3^{(2)}(l) = h_{23}(l) + e_3^{(2)}(l), \quad (3)$$

where  $e_1^{(2)}(l) \sim \mathcal{CN}(0, \gamma)$  and  $e_3^{(2)}(l) \sim \mathcal{CN}(0, \gamma)$  are the corresponding estimation errors.

**Phase 3:** node-3 transmits a pilot symbol  $x = 1$ , which is used by node-1 and node-2 to estimate the channels  $h_{13}(l)$  and  $h_{23}(l)$ , respectively, as

$$\theta_2^{(3)}(l) = h_{23}(l) + e_2^{(3)}(l) \text{ and } \theta_1^{(3)}(l) = h_{13}(l) + e_1^{(3)}(l), \quad (4)$$

where  $e_2^{(3)}(l) \sim \mathcal{CN}(0, \gamma)$  and  $e_1^{(3)}(l) \sim \mathcal{CN}(0, \gamma)$  are the corresponding estimation errors. We assume that all the nodes employ the same channel estimation algorithm, and as a result, we use  $\gamma$  as the variance of the estimation error at all the nodes.

**Phase 4:** By the end of Phase 3, the three nodes have noisy versions of a subset of the intended CSR  $\{h_{12}(l), h_{13}(l)\}$ . Therefore, to fill the gap, in the last phase, node-1 (which acts as the facilitator) transmits the sum  $\theta_1^{(2)}(l) + \theta_1^{(3)}(l)$ , using which node-2 and node-3 receive

$$\begin{aligned}\theta_2^{(4)}(l) &= h_{12}(l) \left( \theta_1^{(2)}(l) + \theta_1^{(3)}(l) \right) + n_2^{(4)}(l), \text{ and} \\ \theta_3^{(4)}(l) &= h_{13}(l) \left( \theta_1^{(2)}(l) + \theta_1^{(3)}(l) \right) + n_3^{(4)}(l),\end{aligned}$$

respectively, where  $n_2^{(4)}(l)$  and  $n_3^{(4)}(l)$  respectively denote the additive noise at node-2 and node-3 distributed as  $\mathcal{CN}(0, \sigma^2)$ . Using  $\theta_2^{(1)}(l)$  and  $\theta_2^{(4)}(l)$ , node-2 learns a noisy version of  $h_{13}(l)$  by first applying a zero-forcing equalizer, and then canceling the known channel realization as

$$\bar{\theta}_2^{(4)}(l) = \left( \left( \theta_2^{(1)}(l) \right)^{-1} \theta_2^{(4)}(l) \right) - \theta_2^{(1)}(l). \quad (5)$$

Similarly, using  $\theta_3^{(1)}(l)$  and  $\theta_3^{(4)}(l)$ , node-3 learns a noisy version of  $h_{12}(l)$  as

$$\bar{\theta}_3^{(4)}(l) = \left( \left( \theta_3^{(1)}(l) \right)^{-1} \theta_3^{(4)}(l) \right) - \theta_3^{(1)}(l). \quad (6)$$

Thus, by the end of Phase 4, the three nodes witness noisy versions of the CSR  $\{h_{12}(l), h_{13}(l)\}$ .

Observe that all the nodes witness noisy version of the CSR, wherein the noise levels depend on the channel realizations in the CSR. Specifically, node-1 observes  $\{h_{12}(l), h_{13}(l)\}$ , which are perturbed by estimation errors. In contrast, node-2 observes  $h_{12}(l)$  under estimation error, however, it observes  $h_{13}(l)$  under both estimation error and the recovery noise during phase 4. Similarly, node-3 has  $h_{13}(l)$ , which is perturbed by estimation error, whereas it has  $h_{12}(l)$ , which is perturbed by both estimation error and the recovery noise during Phase 4.

In terms of leakage, an external eavesdropper receives the following symbols in the four phases:

$$\begin{aligned}y_E^{(1)}(l) &= h_{1E}(l) + n_E^{(1)}(l), y_E^{(2)}(l) = h_{2E}(l) + n_E^{(2)}(l), \\ y_E^{(3)}(l) &= h_{3E}(l) + n_E^{(3)}(l), y_E^{(4)}(l) = h_{1E}(l)(\theta_1^{(2)}(l) + \theta_1^{(3)}(l)) + n_E^{(4)}(l),\end{aligned}$$

where  $h_{jE}$  is the complex channel between node- $j$  for  $1 \leq j \leq 3$  and the eavesdropper, and  $n_E^{(k)}(l)$  is the AWGN at the eavesdropper in Phase  $k$  for  $k = 1, 2, 3, 4$ . Note that the eavesdropper cannot learn the channel realizations  $\{h_{12}(l), h_{13}(l)\}$  during the first three phases by the virtue of its physical location (with the assumption that  $h_{1E}(l), h_{2E}(l), h_{3E}(l)$  are statistically independent of  $h_{12}(l)$  and  $h_{13}(l)$ ). In Phase 4, the CSR continues to be confidential since the sum  $\theta_1^{(2)}(l) + \theta_1^{(3)}(l)$  does not reveal information about either  $\theta_1^{(2)}(l)$  or  $\theta_1^{(3)}(l)$  at the eavesdropper. Overall, the leakage incurred at the eavesdropper is zero.



### III. GROUP SECRET-KEY GENERATION WITH QUANTIZATION

In this section, we discuss some practical aspects of group secret-key generation protocols. In Section II-A, the first three phases involve broadcast of pilot symbols, wherein the receiver nodes estimate the corresponding channels using an appropriate channel estimation algorithm. However, in Phase 4, the sum of the two channel realizations, i.e.,  $\theta_1^{(2)}(l) + \theta_1^{(3)}(l)$ , is transmitted by node-1. Observe that the in-phase and the quadrature components of  $\theta_1^{(2)}(l) + \theta_1^{(3)}(l)$  can be irrational, and as a result, there will be loss of precision when the transmission module of the radio devices are implemented with limited hardware. Furthermore, most practical radios are designed to transmit baseband signals from finite constellations such as Phase Shift Keying (PSK), Quadrature Amplitude Modulation (QAM) etc. Due to such constraints, node-1 would need to transmit a quantized version of the sum  $\theta_1^{(2)}(l) + \theta_1^{(3)}(l)$ , given by

$$\varphi(\theta_1^{(2)}(l) + \theta_1^{(3)}(l)) = \theta_1^{(2)}(l) + \theta_1^{(3)}(l) + z_{sum}(l),$$

where  $\varphi(\cdot)$  is an appropriate quantization algorithm that directly quantizes the channel estimates to points in a complex constellation, denoted by  $\mathcal{A}$ , and  $z_{sum}(l)$  is the corresponding quantization noise. After transmitting the quantized version, the received symbols at node-2 and node-3 are given by

$$\theta_2^4(l) = h_{12}(l) \left( \theta_1^{(2)}(l) + \theta_1^{(3)}(l) + z_{sum}(l) \right) + n_2^{(4)}(l)$$

and

$$\theta_3^4(l) = h_{13}(l) \left( \theta_1^{(2)}(l) + \theta_1^{(3)}(l) + z_{sum}(l) \right) + n_3^{(4)}(l).$$

Using the above received symbols, the channel realizations recovered at node-2 and node-3 are corrupted by the quantization noise in addition to the existing noise in Phase 4. However, in contrast, node-1 views the channel realizations only under the channel estimation errors. Thus, with quantization at node-1, the common randomness across the three nodes are affected by different levels of noise. We refer to the above GSK protocol as Asymmetric Quantized GSK (AQGSK). It is straightforward to verify that  $\theta_1^{(2)}(l) + \theta_1^{(3)}(l) + z_{sum}(l)$  does not leak information on  $\theta_1^{(2)}(l)$  or  $\theta_1^{(3)}(l)$  at the eavesdropper. Although practical, AQGSK suffers from disparity in the effective noise levels at the three nodes. Therefore, we explore new GSK techniques that will help the three nodes increase the key-rate, and yet enable the facilitator (node-1) to transmit symbols from a finite constellation.

### IV. SYMMETRICALLY QUANTIZED GSK (SQGSK)

The quantization noise  $z_{sum}(l)$  that arises by quantizing the sum  $\theta_1^{(2)}(l) + \theta_1^{(3)}(l)$  results in significant noise in the CSR at some of the nodes especially when  $\mathcal{A}$  is small in size. In order to improve the CSR across the three nodes, a straightforward method is to apply quantization on the CSR at the three nodes so

that the quantization noise across the nodes are grossly at the same level. However, a disadvantage with such an idea is asymmetry in the statistics of the quantization noise across the three nodes. To elaborate further, while  $\theta_1^{(2)}(l) + \theta_1^{(3)}(l)$  is quantized at node-1, the noisy version  $\theta_2^{(1)}(l)$  would be quantized at node-2. This way, the statistical distribution of the quantization errors are not identical, which in turn reduces the mutual information across the CSR at the three nodes. To address this issue, we explore an alternate option of individually quantizing  $\theta_1^{(2)}(l)$  and  $\theta_1^{(3)}(l)$ , and then adding their quantized versions at node-1. In such a case,  $z_{sum}(l)$  will be the sum of the quantization errors of  $\theta_1^{(2)}(l)$  and  $\theta_1^{(3)}(l)$ . We refer to this version of AQGSK as AQGSK-II, and refer to the former idea of quantizing the sum  $\theta_1^{(2)}(l) + \theta_1^{(3)}(l)$  (as given in Section III) as AQGSK-I. In the next subsection, we propose a protocol, referred to as Symmetrically Quantized GSK (SQGSK) which reduces the disparity in the noise levels among the CSR at the three nodes.

#### A. Basic Idea

The basic idea behind our strategy is to ensure that the quantization noise at the three nodes are correlated so as to increase the common randomness. Towards that end, we propose the following changes in Phase 4, and use the zero-noise scenario to explain the benefits, i.e., by keeping  $\sigma^2 = 0$  and  $\gamma = 0$ . Without additive noise, the channel estimates across the three nodes would be identical, i.e.,  $\theta_2^{(1)}(l) = \theta_1^{(2)}(l) = h_{12}(l)$ ,  $\theta_3^{(1)}(l) = \theta_1^{(3)}(l) = h_{13}(l)$ , and  $\theta_3^{(2)}(l) = \theta_2^{(3)}(l) = h_{23}(l)$ . As a result, during Phase 4 of each coherence-block, node-1 quantizes the channels  $h_{12}(l)$  and  $h_{13}(l)$  individually, and then adds their quantized versions as  $h_{12}(l) + z_{12}(l) + h_{13}(l) + z_{13}(l)$ , where  $z_{12}(l)$  and  $z_{13}(l)$  are the corresponding quantization errors of  $h_{12}(l)$  and  $h_{13}(l)$ , respectively. Due to this operation, the transmitted symbol from node-1 takes values from the set  $\mathcal{A} \oplus \mathcal{A} \subset \mathbb{C}$ , which is still a finite constellation. The received baseband signals at node-2 and node-3 in Phase 4 are given by

$$\theta_2^{(4)}(l) = h_{12}(l) (h_{12}(l) + h_{13}(l) + z_{13}(l) + z_{12}(l)) \quad \text{and} \quad (7)$$

$$\theta_3^{(4)}(l) = h_{13}(l) (h_{12}(l) + h_{13}(l) + z_{13}(l) + z_{12}(l)). \quad (8)$$

From Phase 1, node-2 has perfect knowledge of  $h_{12}(l)$ . Using that in (7), node-2 will recover  $h_{12}(l) + h_{13}(l) + z_{13}(l) + z_{12}(l)$ , and then subtract it by the quantized version of  $h_{12}(l)$ , i.e.,  $h_{12}(l) + z_{12}(l)$ , thereby completely canceling the quantization noise  $z_{12}(l)$ . Similarly, node-3 will subtract the quantized version of  $h_{13}(l)$  from  $h_{12}(l) + h_{13}(l) + z_{13}(l) + z_{12}(l)$ , thereby completely canceling the quantization noise  $z_{13}(l)$ . After the above operations, it is straightforward to observe that the CSR observed at the three nodes is  $\{h_{12}(l) + z_{12}(l), h_{13}(l) + z_{13}(l)\}$ . Taking insights from the above discussion, we elaborate on different phases of the SQGSK protocol in the next section.

## B. SQGSK Protocol

To start with, the three nodes agree upon a finite complex constellation  $\mathcal{A} \subset \mathbb{C}$ , given by  $\mathcal{A} = \mathcal{A}_I \oplus i\mathcal{A}_Q$  such that  $\mathcal{A}_I = \mathcal{A}_Q$ . The proposed protocol comprises of four phases as described below:

**Phase 1:** node-1 transmits a pilot symbol  $x = 1$ , which is used by node-2 and node-3 to estimate the channels  $h_{12}(l)$  and  $h_{13}(l)$ , respectively. Further, these values are quantized to the values in the constellation  $\mathcal{A}$  as

$$\theta_2^{(1)}(l) = \varphi(h_{12}(l) + e_2^{(1)}(l)), \theta_3^{(1)}(l) = \varphi(h_{13}(l) + e_3^{(1)}(l)),$$

where  $\varphi(\cdot)$  is the quantization operator that works independently on the in-phase and the quadrature components by mapping them to the nearest points in  $\mathcal{A}_X$  for  $X \in \{I, Q\}$ . Specifically, for  $x \sim \mathcal{N}(0, \Sigma)$ , we have

$$\varphi(x) = \arg \min_{a \in \mathcal{A}_I} |x - a|^2. \quad (9)$$

**Phase 2:** node-2 transmits a pilot symbol  $x = 1$ , which is used by node-1 and node-3 to estimate and then quantize the channels  $h_{12}(l)$  and  $h_{23}(l)$ , respectively as

$$\theta_1^{(2)}(l) = \varphi(h_{12}(l) + e_1^{(2)}(l)), \theta_3^{(2)}(l) = \varphi(h_{23}(l) + e_3^{(2)}(l)).$$

**Phase 3:** node-3 transmits a pilot symbol  $x = 1$ , which is used by node-1 and node-2 to estimate the channels  $h_{13}(l)$  and  $h_{23}(l)$ , respectively. Further, these values are quantized to the values in the constellation  $\mathcal{A}$  as

$$\theta_1^{(3)}(l) = \varphi(h_{13}(l) + e_3^{(3)}(l)), \theta_2^{(3)}(l) = \varphi(h_{23}(l) + e_2^{(3)}(l)).$$

**Phase 4:** In the last phase, node-1 transmits the sum  $\theta_1^{(2)}(l) + \theta_1^{(3)}(l)$ , using which node-2 and node-3 receive

$$\theta_2^{(4)}(l) = h_{12}(l)(\theta_1^{(2)}(l) + \theta_1^{(3)}(l)) + n_2^{(4)}(l),$$

and

$$\theta_3^{(4)}(l) = h_{13}(l)(\theta_1^{(2)}(l) + \theta_1^{(3)}(l)) + n_3^{(4)}(l),$$

respectively. Since node-2 has the knowledge of both  $h_{12}(l) + e_2^{(1)}(l)$  and  $\varphi(h_{12}(l) + e_2^{(1)}(l))$ , it recovers a noisy version of  $\varphi(h_{13}(l))$  by first applying a zero-forcing equalizer and subsequently canceling the quantized version as

$$\bar{\theta}_2^4(l) = \left( h_{12}(l) + e_2^{(1)}(l) \right)^{-1} \theta_2^{(4)}(l) - \varphi \left( h_{12}(l) + e_2^{(1)}(l) \right). \quad (10)$$

Similarly, node-3 obtains a noisy version of  $\varphi(h_{12}(l))$  as

$$\bar{\theta}_3^4(l) = \left( h_{13}(l) + e_3^{(1)}(l) \right)^{-1} \theta_3^{(4)}(l) - \varphi \left( h_{13}(l) + e_3^{(1)}(l) \right). \quad (11)$$

Thus, the CSR seen by node-1, node-2 and node-3 are

$$\left\{ \varphi \left( h_{12}(l) + e_1^{(2)}(l) \right), \varphi \left( h_{13}(l) + e_1^{(3)}(l) \right) \right\},$$

$$\left\{ \varphi \left( h_{12}(l) + e_2^{(1)}(l) \right), \bar{\theta}_2^4(l) \right\} \text{ and } \left\{ \bar{\theta}_3^4(l), \varphi \left( h_{13}(l) + e_3^{(1)}(l) \right) \right\},$$

respectively, where  $\bar{\theta}_2^4(l)$  and  $\bar{\theta}_3^4(l)$  are as given in (10) and (11).

With respect to the channel  $h_{12}(l)$ , it is clear that the common randomness is hampered by that of node-3 due to the recovery noise in Phase 4. Similarly, the common randomness from the channel  $h_{13}(l)$  is hampered by that of node-2 due to recovery noise in Phase 4.

### C. Secret-Key Rate of the SQGSK Protocol

In this section, we show that the key-rate with SQGSK is higher than the AQGSK-II protocol under the scenario when the channel estimates at all the nodes are assumed to be perfect in the first three phases. The objective here is to bring out the difference between SQGSK and AQGSK-II during Phase 4, which mainly caters to recovering the channel estimates of the adjacent channels. We have chosen AGQSK-II as the relevant baseline to compare the key-rate of SQGSK as both protocols use the same constellation  $\mathcal{A} \oplus \mathcal{A}$  to transmit the baseband symbols by the facilitator, node-1. In contrast, comparison with AQGSK-I is not fair given that the facilitator uses  $\mathcal{A}$  for transmitting baseband symbols in Phase 4.

*Proposition 1:* With perfect channel estimates in the first three phases, the key-rate offered by SQGSK protocol is higher than the AQGSK-II protocol.

*Proof:* With perfect estimates of the direct channels,  $\gamma = 0$  will apply in the first three phases. Since we are addressing the impact of the recovery noise in Phase 4, we only consider the recovery process of  $h_{12}(l)$  at node-3. A similar argument is also applicable for recovering  $h_{13}(l)$  at node-2, and hence we omit that case. In the rest of this proof, we discard the reference to index  $l$ . The channel  $h_{12}$  goes through the following modifications:

$$h_{12} \rightarrow h_{12} + z_{12} \rightarrow h_{12} + z_{12} + z_{13} \rightarrow h_{12} + z_{12} + z_{13} + h_{13}^{-1}n_3^{(4)},$$

where the first modification is at node-1, the next is after subtracting  $h_{12}$  at node-3, and the final one is the effect of the additive noise at node-3. Due to Markov-chain property on the above sequence, we have the upper bound in (12), given by

$$I \left( h_{12}; h_{12} + z_{12} + z_{13} + h_{13}^{-1}n_3^{(4)} \right) \leq I \left( h_{12} + z_{12}; h_{12} + z_{12} + z_{13} + h_{13}^{-1}n_3^{(4)} \right). \quad (12)$$

Furthermore, the Markov chain

$$h_{12} + z_{12} \rightarrow h_{12} + z_{12} + z_{13} \rightarrow h_{12} + z_{12} + z_{13} + h_{13}^{-1}n_3^{(4)}$$

can be re-written as

$$h_{12} + z_{12} \rightarrow h_{12} + z_{12} + h_{13}^{-1}n_3^{(4)} \rightarrow h_{12} + z_{12} + h_{13}^{-1}n_3^{(4)} + z_{13}.$$

Thus, we have the inequality in (13), given by

$$I\left(h_{12} + z_{12}; h_{12} + z_{12} + z_{13} + h_{13}^{-1}n_3^{(4)}\right) \leq I\left(h_{12} + z_{12}; h_{12} + z_{12} + h_{13}^{-1}n_3^{(4)}\right). \quad (13)$$

Finally, we have (14), given by

$$I\left(h_{12}; h_{12} + z_{12} + z_{13} + h_{13}^{-1}n_3^{(4)}\right) \leq I\left(h_{12} + z_{12}; h_{12} + z_{12} + h_{13}^{-1}n_3^{(4)}\right). \quad (14)$$

by combining (12) and (13). Using (1), we highlight that the mutual information given on the right hand side of (14) dictates the key-rate generated by the SQGSK protocol. ■

#### D. Confidentiality of the CSR in SQGSK protocol

With the use of finite constellation, the noisy version of the CSR witnessed at node-1 takes values from  $\mathcal{A}$ . Due to this discrete nature, an external eavesdropper, although unable to directly witness the CSR  $\{h_{12}(l), h_{13}(l)\}$ , can construct several candidates for  $h_{12}(l)$  and  $h_{13}(l)$  by listening to the symbol transmitted by node-1 in Phase 4. Specifically, the number of such candidates depends on the received value  $\theta_1^2(l) + \theta_1^3(l)$ ; this is because, more than two pairs from  $\mathcal{A} \times \mathcal{A}$  may result in the same value in  $\mathcal{A} \oplus \mathcal{A}$  [24]. In the rest of this section, we present leakage analysis at the eavesdropper assuming that she has no additive noise, thereby capturing worst-case leakage.

*Theorem 1:* With regular  $M$ -QAM constellation as  $\mathcal{A}$ , we have  $I(\theta_1^2(l); \theta_1^2(l) + \theta_1^3(l)) > 0$ , where  $\theta_1^2(l) + \theta_1^3(l)$  is the symbol transmitted by node-1 in Phase 4 of the SQGSK protocol.

*Proof:* In Phase 4 of the coherence-block  $l$ , the received symbol at the eavesdropper is given by

$$y_E^{(4)}(l) = h_{1E}(l) (\theta_1^2(l) + \theta_1^3(l)) + n_E^{(4)}(l),$$

where  $h_{1E}(l)$  is the complex channel between node-1 and the eavesdropper, and  $n_E^{(4)}(l) \sim \mathcal{CN}(0, \Omega)$  is the AWGN noise at the eavesdropper. We assume the worst-case scenario that  $\Omega = 0$ , and also assume that the eavesdropper perfectly knows the channel  $h_{1E}$ . As a result, the eavesdropper can perfectly recover the transmitted point  $\theta_1^2(l) + \theta_1^3(l) \in \mathcal{A} \oplus \mathcal{A}$ . We prove the theorem statement by contradiction. Suppose,  $I(\theta_1^2(l); \theta_1^2(l) + \theta_1^3(l)) = 0$ . This implies that  $H(\theta_1^2(l) | \theta_1^2(l) + \theta_1^3(l) = \theta(l)) = H(\theta_1^2(l))$  with  $|\mathcal{A}|$  mass points on the conditional PMF  $P(\theta_1^2(l) | \theta_1^2(l) + \theta_1^3(l) = \theta(l))$ , for every  $\theta(l) \in \mathcal{A} \oplus \mathcal{A}$ . However, with any regular  $M$ -QAM constellation, it is straightforward to pick a point in  $\theta(l) \in \mathcal{A} \oplus \mathcal{A}$  such that  $P(\theta_1^2(l) | \theta_1^2(l) + \theta_1^3(l) = \theta(l))$  is one, and this is a contradiction. This completes the proof. ■

We attempt to fix the above limitation of the SQGSK protocol by introducing the following modifications: In Phase 4 of each coherence-block, node-1 transmits 0 when  $\theta_1^2(l)$  and  $\theta_1^3(l)$  are uniquely

recoverable from  $\theta_1^2(l) + \theta_1^3(l)$ ; this case corresponds to the scenario when  $\theta_1^2(l)$  and  $\theta_1^3(l)$  are identical, and take points that have maximum energy in  $M$ -QAM. In order to help node-2 and node-3 distinguish this from the other cases where  $\theta_1^2(l) + \theta_1^3(l) = 0$ , in the consensus phase of the SQGSK protocol, node-1 discards all those index values which correspond to the coherence-blocks when  $\theta_1^2(l)$  and  $\theta_1^3(l)$  are uniquely recoverable from  $\theta_1^2(l) + \theta_1^3(l)$ . We refer to this version of the SQGSK protocol as the optimized SQGSK protocol. To quantify the leakage associated with the SQGSK protocols, we define residual entropy  $\eta$  at the eavesdropper as

$$\eta = \frac{H(\theta_1^2(l) | \theta_1^2(l) + \theta_1^3(l))}{H(\theta_1^2(l))} \times 100.$$

In Fig. 4, we plot  $\eta$  for both SQGSK and optimized SQGSK with 4-, 16- and 64-QAM. To study the leakage effect, we also scale the QAM constellations by using a scale factor  $\alpha$ , because shrinking or enlarging  $\mathcal{A}$  changes  $H(\theta_1^2(l))$ ; this is attributed to the fact that the distribution of  $h_{12}(l) + e_1^{(2)}(l)$  is fixed. We observe that with  $\alpha > 1$ , the effective constellation  $\frac{\mathcal{A}}{\alpha}$  shrinks, and as a result dropping the uniquely recoverable points increases the residual entropy at the eavesdropper. However, on the other hand, with  $\alpha = 1$ , the residual entropy of optimized SQGSK approximately matches that of SQGSK since the probability associated with the uniquely recoverable points vanishes to zero. Fig. 4 shows that the benefits of optimized SQGSK is significant (from 50% to 75%) with 4-QAM since the probability associated with the uniquely recoverable points is non-negligible. However, as the size of the constellation grows from 16-QAM to 64-QAM, the benefits of optimized SQGSK reduce. Overall, despite diminishing returns of optimized SQGSK over the SQGSK protocol, the plots in Fig. 4 show that SQGSK protocols incur significant leakage of the CSR.

## V. ALGEBRAIC SQGSK PROTOCOL

In this section, we propose a new practical GSK protocol which compensates the leakage drawbacks of SQGSK. The central idea behind this method is to avoid transmitting symbols in  $\mathcal{A} \oplus \mathcal{A}$ . Instead, the quantized values  $\theta_1^2(l)$  and  $\theta_1^3(l)$  at node-1 are appropriately transformed to points in an algebraic ring, and are then added in the ring. Subsequently, the outcome of the *addition operation* in the ring is mapped back to a point in  $\mathcal{A}$  before transmission. For example, see Fig. 5 which captures this idea when using 16-QAM as  $\mathcal{A}$ . We refer to this method as the Algebraic SQGSK protocol. Since the transmitted baseband symbol by node-1 belongs to  $\mathcal{A}$ , we consider AQGSK-I as the relevant baseline to this protocol. The specific ingredients needed for the Algebraic SQGSK protocol are given below.

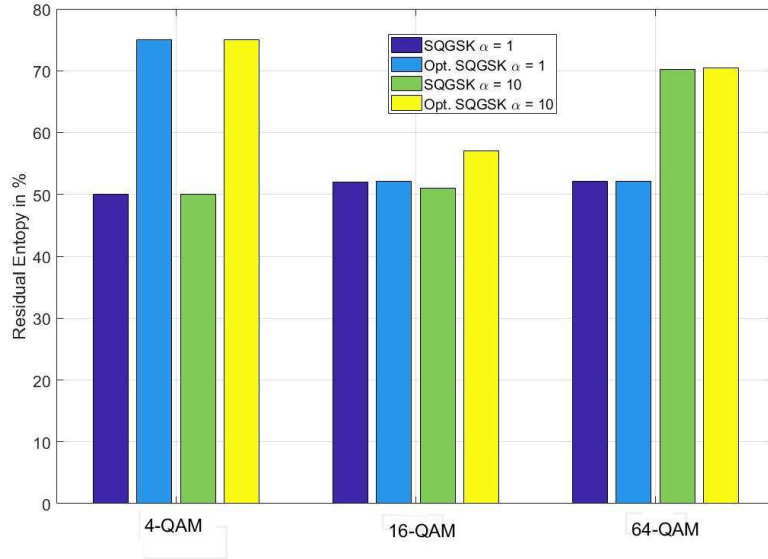


Fig. 4. Leakage associated with SQGSK and optimized SQGSK when used along with 4-, 16- and 64-QAM.

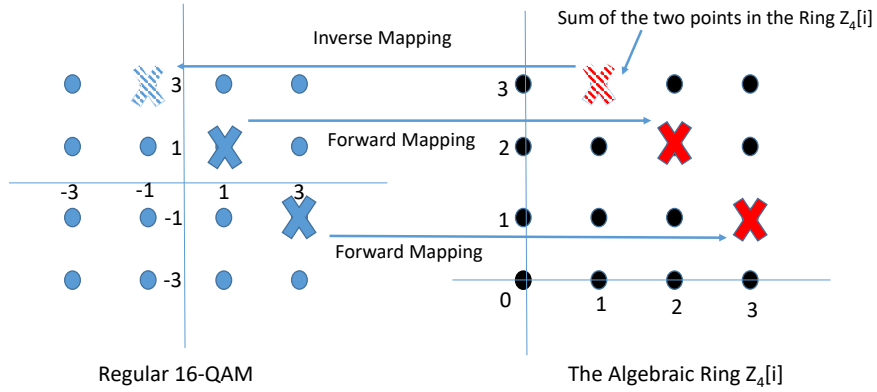


Fig. 5. Depiction of algebraic operations by translating the regular  $2^m$ -QAM constellation to  $\mathbb{Z}_{\frac{m}{2}}[i]$  with  $m = 4$ .

### A. Ingredients

A regular  $2^m$ -QAM constellation  $\mathcal{A}$ , where  $m$  is even, given by

$$\mathcal{A} = \mathcal{A}_I \oplus i\mathcal{A}_Q,$$

such that  $\mathcal{A}_I = \mathcal{A}_Q = \{-2^{\frac{m}{2}} + 1, -2^{\frac{m}{2}} + 3, \dots, 2^{\frac{m}{2}} - 3, 2^{\frac{m}{2}} - 1\}$ , can be written as a scaled and shifted version of the constellation  $\bar{\mathcal{A}} = \{0, 1, \dots, 2^{\frac{m}{2}} - 1\} \oplus \{0, i, \dots, i(2^{\frac{m}{2}} - 1)\}$ , where  $i = \sqrt{-1}$ . In particular,  $\bar{\mathcal{A}}$  forms an algebraic ring  $\mathbb{Z}_{2^{\frac{m}{2}}}[i]$ , defined over regular addition and multiplication, however, with modulo  $2^{\frac{m}{2}}$  operation on both the in-phase and the quadrature components. We represent the transformation from  $\mathcal{A}$  to  $\bar{\mathcal{A}}$  by  $\phi : \mathcal{A} \rightarrow \bar{\mathcal{A}}$ , where

$$\phi(x) = \frac{x + 2^{\frac{m}{2}} - 1 + i(2^{\frac{m}{2}} - 1)}{2}, \quad (15)$$

for  $x \in \mathcal{A}$ .

*Proposition 2:* The transformation  $\phi$  in (15) is one-one.

*Proposition 3:* The constellation  $\bar{\mathcal{A}}$  forms a commutative group under addition, where addition of  $x, y \in \bar{\mathcal{A}}$  is defined as

$$x + y = ((\mathbf{I}(x) + \mathbf{I}(y)) \bmod 2^{\frac{m}{2}}) + i((\mathbf{Q}(x) + \mathbf{Q}(y)) \bmod 2^{\frac{m}{2}}),$$

such that  $\mathbf{I}(x)$  and  $\mathbf{Q}(x)$  denote the in-phase and quadrature components of the complex number  $x$ , and  $\mathbf{I}(y)$  and  $\mathbf{Q}(y)$  denote the in-phase and quadrature components of the complex number  $y$ .

*Example 1:* For the 16-QAM constellation as shown in Fig. 5, the transformation  $\phi : \mathcal{A} \rightarrow \bar{\mathcal{A}}$  is given by  $\phi(x) = \frac{x}{2} + 1.5 + 1.5i$  for  $x \in \mathcal{A}$ .

In the next subsection, we use the transformation  $\phi$  in Phase 4 of the SQGSK protocol to obtain the Algebraic SQGSK scheme.

### B. Algebraic SQGSK Protocol

Similar to the SQGSK protocol, the three nodes agree upon a regular  $M$ -QAM for  $\mathcal{A}$ , where  $M = 2^m$  such that  $m$  is even. Furthermore, the first three phases are identical to that of SQGSK protocol, and therefore we only explain the last phase.

**Phase 4:** In the last phase, node-1 applies the transformation  $\phi(\cdot)$  on  $\theta_1^{(2)}(l)$  and  $\theta_1^{(3)}(l)$  to obtain  $\phi(\theta_1^{(2)}(l)) \in \bar{\mathcal{A}}$  and  $\phi(\theta_1^{(3)}(l)) \in \bar{\mathcal{A}}$ , respectively. Subsequently, node-1 computes

$$\theta_{sum}(l) = \phi(\theta_1^{(2)}(l)) + \phi(\theta_1^{(3)}(l)) \in \bar{\mathcal{A}},$$

where the addition is over the ring  $\mathbb{Z}_{2^{\frac{m}{2}}}[i]$ , and then it broadcasts  $\theta(l) \triangleq \phi^{-1}(\theta_{sum}(l)) \in \mathcal{A}$  to node-2 and node-3. Here  $\phi^{-1}(\cdot)$  denotes the inverse of the transformation  $\phi$ . With this, the received symbols at node-2 and node-3 are given by  $\theta_2^{(4)}(l) = h_{12}(l)\theta(l) + n_2^{(4)}(l)$ , and  $\theta_3^{(4)}(l) = h_{13}(l)\theta(l) + n_3^{(4)}(l)$ , respectively.



Since node-2 has the knowledge of both  $h_{12}(l) + e_2^{(1)}(l)$  and  $\varphi(h_{12}(l) + e_2^{(1)}(l))$ , it obtains an estimate  $\hat{\theta}(l)$  using the MAP decoder<sup>2</sup> given by

$$\hat{\theta}(l) = \arg \max_{a_j \in \mathcal{A}} \left( e^{-\frac{|\theta_2^{(4)}(l) - (h_{12}(l) + e_2^{(1)}(l))a_j|^2}{\sigma^2}} P(\theta(l) = a_j) \right), \quad (16)$$

where  $P(\theta(l) = a_j)$  is the probability that the random variable  $\theta(l)$  takes the value  $a_j \in \mathcal{A}$ . Using the above estimate, node-2 obtains an estimate of the quantized version of  $h_{13}(l)$  as

$$\bar{\theta}_2^4(l) = \phi^{-1} \left( \phi(\hat{\theta}(l)) - \phi(\varphi(h_{12}(l) + e_2^{(1)}(l))) \right), \quad (17)$$

where the subtraction is over the ring  $\mathbb{Z}_{\frac{m}{2}}[i]$ . Similarly, node-3 obtains an estimate of the quantized version of  $h_{12}(l)$  as

$$\bar{\theta}_3^4(l) = \phi^{-1} \left( \phi(\hat{\theta}(l)) - \phi(\varphi(h_{13}(l) + e_3^{(1)}(l))) \right). \quad (18)$$

Thus, the CSR seen by node-1, node-2 and node-3 are

$$\left\{ \varphi \left( h_{12}(l) + e_1^{(2)}(l) \right), \varphi \left( h_{13}(l) + e_1^{(3)}(l) \right) \right\}, \\ \left\{ \varphi \left( h_{12}(l) + e_2^{(1)}(l) \right), \bar{\theta}_2^4(l) \right\}, \text{ and } \left\{ \bar{\theta}_3^4(l), \varphi \left( h_{13}(l) + e_3^{(1)}(l) \right) \right\},$$

respectively, where  $\bar{\theta}_2^4(l)$  and  $\bar{\theta}_3^4(l)$  are as given in (17) and (18). Unlike SQGSK, the CSR witnessed at the three nodes belong to the constellation  $\mathcal{A}$ .

### C. Key-Rate Comparison with AQGSK-I

In order to capture the effect of quantization noise, we compare Algebraic SQGSK and AQGSK-I with no additive noise. With no additive noise, i.e., when  $\sigma^2 = 0$  and  $\gamma = 0$ , it is straightforward to verify that the CSR at the three nodes in Algebraic SQGSK protocol will be  $\{h_{12}(l) + z_1(l), h_{13}(l) + z_2(l)\}$ , where  $z_1(l)$  and  $z_2(l)$  are the quantization errors corresponding to  $h_{12}(l)$  and  $h_{13}(l)$ , respectively. By applying the information-theoretic result in (1), the secret-key rate when using  $h_{12}(l)$  as the CSR is determined by

$$K_{A-SQGSK} = \frac{1}{4} H(h_{12}(l) + z_1(l)), \quad (19)$$

where  $K_{A-SQGSK}$  can be numerically computed using the PMF on the discrete random variable  $h_{12}(l) + z_1(l) \in \mathcal{A}$ . Specifically, since  $h_{12}(l)$  is a complex Gaussian random variable, the PMF on  $h_{12}(l) + z_1(l)$  can be computed using standard  $Q(\cdot)$  function, where  $Q(x) = \frac{1}{\sqrt{2\pi}} \int_{t=x}^{\infty} \exp(-\frac{t^2}{2}) dt$ . In contrast, under the same scenario, when using AQGSK-I the CSR at node-1, node-2 and node-3 are  $\{h_{12}(l), h_{13}(l)\}$ ,  $\{h_{12}(l), h_{13}(l) + z_{sum}(l)\}$ , and  $\{h_{12}(l) + z_{sum}(l), h_{13}(l)\}$ , respectively, where  $z_{sum}(l)$  is the quantization

<sup>2</sup>Since the probability mass function on the points in the constellation  $\mathcal{A}$  is not uniform, maximum likelihood (ML) decoder is not optimal in this case.

noise resulting from quantizing the sum  $h_{12}(l) + h_{13}(l)$  to a point in  $\mathcal{A}$  by node-1. In this case, by applying (1), the secret-key rate  $K_{AQGSK-I}$  when using  $h_{12}(l)$  is given by

$$\begin{aligned} & \frac{1}{4} \min(H(h_{12}(l)), I(h_{12}(l); h_{12}(l) + z_{sum}(l) | h_{13}(l))) \\ & = \frac{1}{4} I(h_{12}(l); h_{12}(l) + z_{sum}(l) | h_{13}(l)), \end{aligned} \quad (20)$$

where the equality is applicable by the definition of mutual information and the assumption that  $h_{12}(l)$  and  $h_{13}(l)$  are statistically independent. Furthermore, we have

$$\begin{aligned} K_{AQGSK-I} & \leq \frac{1}{4} H(h_{12}(l) + z_{sum}(l) | h_{13}(l)) \\ & = \frac{1}{4} H(h_{12}(l) + h_{13}(l) + z_{sum}(l) | h_{13}(l)), \end{aligned} \quad (21)$$

where the equality follows from the identity that differential entropy is invariant to translation of the random variable by a constant. Note that the conditional entropy  $H(h_{12}(l) + h_{13}(l) + z_{sum}(l) | h_{13}(l))$  can be numerically evaluated by using the conditional PMF on the discrete random variable  $h_{12}(l) + h_{13}(l) + z_{sum} \in \mathcal{A}$ . We now show through numerical evaluation that the key-rate offered by  $K_{A-SQGSK}$  is higher than  $K_{AQGSK-I}$ . In Fig. 6, we use 4-QAM, 16-QAM, and 64-QAM as  $\mathcal{A}$  to compare  $K_{A-SQGSK}$  in (19) and the upper bound on  $K_{AQGSK-I}$  given in (21) by keeping the average transmit power at node-1 identical between the two schemes. The plots in Fig. 6 show that the Algebraic SQGSK outperforms AQGSK-I when  $\sigma^2 = 0$ .

We caution the reader that the no additive-noise scenario is used to capture the effect of quantization noise. However, in Section VI, we use extensive simulation results to show that the Algebraic-SQGSK continues to outperform AQGSK-I when  $\sigma^2 \neq 0$  and  $\gamma \neq 0$ .

#### D. Confidentiality of the CSR in Algebraic SQGSK

In this section, we prove that the Algebraic SQGSK protocol does not leak the CSR to an external eavesdropper.

*Theorem 2:* With regular  $2^m$ -QAM constellation, we have  $I(\theta_1^{(2)}(l); \theta(l)) = 0$ , where  $\theta(l)$  is the symbol transmitted by node-1 in Phase 4 of the Algebraic SQGSK protocol.

*Proof:* In Phase 4 of the coherence-block  $l$ , the received symbol at the eavesdropper is given by

$$y_E^{(4)}(l) = h_{1E}(l) (\theta(l)) + n_E^{(4)}(l),$$

where  $h_{1E}(l)$  is the complex channel between node-1 and the eavesdropper, and  $n_E^{(4)}(l) \sim \mathcal{CN}(0, \Omega)$  is the AWGN noise at the eavesdropper. In this leakage analysis, we assume the worst-case scenario that  $\Omega = 0$ , and also assume that the eavesdropper perfectly knows the channel  $h_{1E}(l)$  (using Phase 1 of the

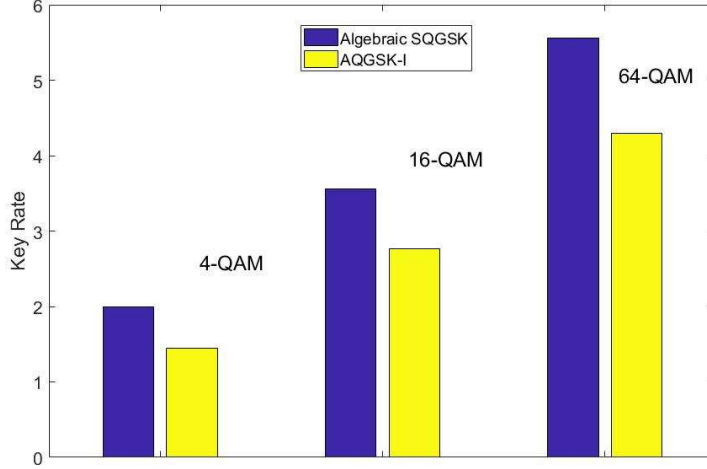


Fig. 6. Comparison between the key-rate of Algebraic SQGSK in (19) and the upper bound on the key-rate of AQS-GSK-I in (21) under no additive-noise scenario. We have omitted the scalar  $\frac{1}{4}$  from (19) and (21) when plotting the above figure. For a fair comparison, the average transmit power at node-1 in Phase 4 is held constant between the two schemes. The plots show that Algebraic SQGSK outperforms AQS-GSK-I.

protocol). As a result, the eavesdropper can perfectly recover the transmitted point  $\theta(l) \in \mathcal{A}$  by node-1. We now analyze the conditional entropy  $H(\theta_1^2(l) | \theta(l))$ , which quantifies the residual entropy at the eavesdropper. Formally, we have

$$H(\theta_1^2(l) | \theta(l)) = - \sum_{j=1}^M H(\theta_1^2(l) | \theta(l) = c_j) P(\theta(l) = c_j),$$

where  $P(\theta(l) = c_j)$  is the probability that the random variable  $\theta(l)$  takes the realization  $c_j \in \mathcal{A}$ , and  $H(\theta_1^2(l) | \theta(l) = c_j)$  is given by

$$H(\theta_1^2(l) | \theta(l) = c_j) = - \sum_{k=1}^M P(\theta_1^2(l) = b_k | \theta(l) = c_j) \log_2(P(\theta_1^2(l) = b_k | \theta(l) = c_j)), \quad (22)$$

where  $P(\theta_1^2(l) = b_k | \theta(l) = c_j)$  is the conditional probability that the random variable  $\theta_1^2(l)$  takes the realization  $b_k \in \mathcal{A}$  conditioned that  $\theta(l) = c_j$ . We immediately note that

$$P(\theta_1^2(l) = b_k | \theta(l) = c_j) = P(\theta_1^3(l) = \phi^{-1}(\phi(c_j) - \phi(b_k)))$$

where the subtraction is over the ring  $\mathbb{Z}_{2^{\frac{m}{2}}}[i]$ . Since  $c_j$  is fixed, the symbol  $\phi^{-1}(\phi(c_j) - \phi(b_k))$  results in a distinct value of  $\mathcal{A}$  for each value of  $b_k$ . Therefore, we have the equality

$$H(\theta_1^2(l) | \theta(l) = c_j) = H(\theta_1^3(l)),$$

and thus we have

$$H(\theta_1^2(l) | \theta(l)) = H(\theta_1^3(l)).$$

TABLE I  
AN EXHAUSTIVE COMPARISON OF VARIOUS PRACTICAL GSK GENERATION PROTOCOLS

Parameters	AQGSK-I	AQGSK-II	SQGSK	Algebraic SQGSK
Nature of the CSR $h_{12}$ at node-1	continuous	continuous	discrete	discrete
Nature of the CSR $h_{12}$ at node-2	continuous	continuous	discrete	discrete
Nature of the CSR $h_{12}$ at node-3	continuous	continuous	continuous	discrete
Nature of the CSR $h_{13}$ at node-1	continuous	continuous	discrete	discrete
Nature of the CSR $h_{13}$ at node-2	continuous	continuous	continuous	discrete
Nature of the CSR $h_{13}$ at node-3	continuous	continuous	discrete	discrete
Transmitted constellation at node-1	$\mathcal{A}$	$\mathcal{A} \oplus \mathcal{A}$	$\mathcal{A} \oplus \mathcal{A}$	$\mathcal{A}$
Leakage		non-zero	non-zero	zero
Key-rate	low	low	higher than AQGSK-II	higher than AQGSK-I

Since  $h_{12}(l) + e_1^2(l)$  and  $h_{13}(l) + e_1^3(l)$  are identically distributed, we have  $H(\theta_1^{(3)}(l)) = H(\theta_1^{(2)}(l))$ , and therefore, we have  $H(\theta_1^{(2)}(l) | \theta(l)) = H(\theta_1^{(2)}(l))$ . This completes the proof. ■

The above theorem has shown that Algebraic SQGSK does not leak the CSR to an external eavesdropper, thereby fixing the drawback of the SQGSK protocol. Overall, to summarize the differences between the proposed protocols, Table I provides an exhaustive comparison of the nature of CSR observed when using the practical GSK generation protocols.

## VI. SIMULATION RESULTS WITH SQGSK PROTOCOLS

In this section, we present simulation results to demonstrate the performance of the proposed protocols in terms of key-rate, which is defined as the average number of secret bits generated per coherence-block. To generate the results, we apply both SQGSK and Algebraic SQGSK protocols in conjunction with the well known level-crossing algorithm [1]. The signal model for the three-node network is as described in Section II. In the first three phases of the protocol, all the nodes use the received symbols as the noisy estimates of the channel realizations, i.e.,  $\gamma = \sigma^2$ . The constellation  $\mathcal{A} \subset \mathbb{C}$  used in the simulations are regular 4-QAM, 16-QAM and 64-QAM. We use  $L = 1000$  coherence-blocks, after which each node generates 4000 real samples as input to the key generation algorithm. Out of the 4000 samples, the first 2000 correspond to the in-phase and quadrature components of  $\{h_{12}(l) | 1 \leq l \leq 1000\}$  arranged as

$$\{\mathbf{I}(h_{12}(1)), \mathbf{Q}(h_{12}(1)), \dots, \mathbf{I}(h_{12}(1000)), \mathbf{Q}(h_{12}(1000))\},$$

where  $\mathbf{I}(x)$  and  $\mathbf{Q}(x)$  denote the in-phase and quadrature component of a complex number  $x$ , respectively. Similarly, the other half corresponds to the in-phase and quadrature components of  $\{h_{13}(l) | 1 \leq l \leq$

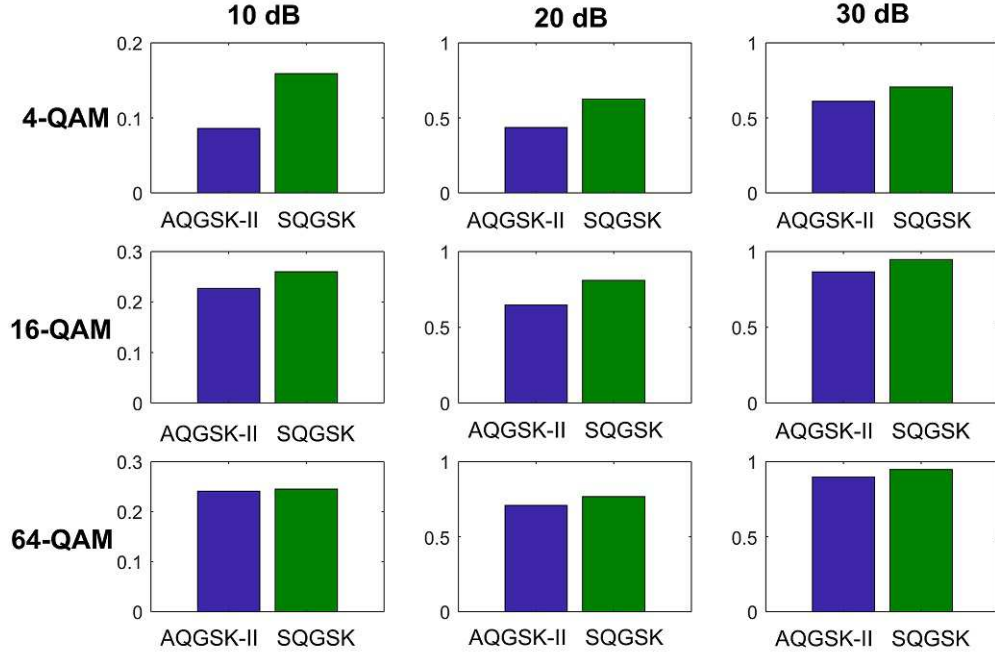


Fig. 7. Key-rate comparison between AQGSK-II and SQGSK against various SNR values and complex constellations. The excursion-length and the threshold levels of the key generation algorithm are varied to keep the same bit-error-rate for AQGSK-II and SQGSK. To generate the above results, BER was held at 5%, 2% and 1% at 10 dB, 20 dB and 30 dB, respectively.

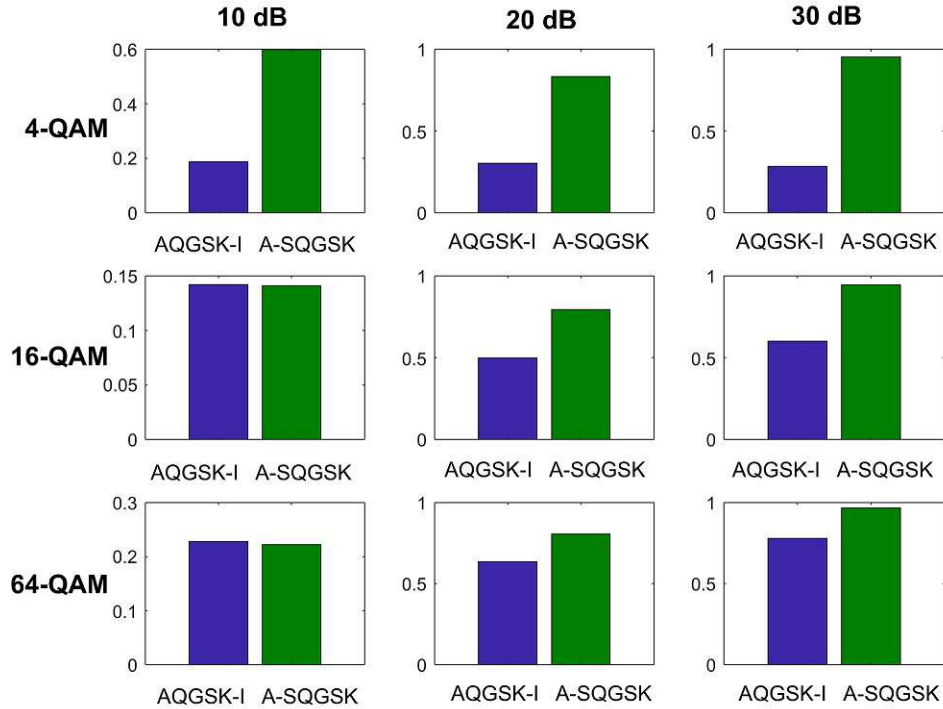


Fig. 8. Key-rate comparison between AQGSK-I and Algebraic SQGSK against various SNR values and  $M$ -QAM constellations. The excursion-length and the threshold levels of the key generation algorithm are varied to keep the same bit-error-rate for AQGSK-I and Algebraic SQGSK. To generate the above results, BER was held at 5%, 2% and 1% at 10 dB, 20 dB and 30 dB, respectively.

1000}. Since the effective noise experienced by the three nodes are at different levels, each node deploys the level-crossing algorithm by choosing the threshold levels as a function of its effective noise.

An important component of the key generation algorithm is the consensus phase, which happens over the public channel. The order of exchanging information for consensus depends on the channel realization in our protocol. With respect to  $\{h_{12}(l)\}$ , node-1 first generates the index values of samples that represent the center of excursions, and then broadcasts them. Subsequently, node-2 picks a subset of those index values which also abides by the excursion length, and then broadcasts the shortlisted index values. Since node-3 is the weakest in terms of the effective noise, it finalizes the list of index values based on the its samples, and broadcasts the list of final index values. In the end, each node generates a binary secret-key by quantizing the samples on the final list of index values. The consensus protocol for the channel realizations  $\{h_{13}(l)\}$  is similar to that of  $\{h_{12}(l)\}$ , however, this time the consensus order is node-1  $\rightarrow$  node-3  $\rightarrow$  node-2, since node-2 is the weakest in the terms of the effective noise. By the end of the consensus phase, it is possible that the digital keys generated at the three nodes differ in few locations, and this results in errors in the group secret-key.

#### A. Baselines and Results

With the above ingredients, the key-rate of the SQGSK protocol and the Algebraic SQGSK protocol are presented in Fig. 7 and Fig. 8, respectively. Here, key-rate is computed by dividing the length of the generated key by  $L = 1000$ . In Fig. 7, the key-rate of the SQGSK protocol is compared with AQGSK-II, wherein  $h_{12}(l) + e_1^{(2)}(l)$  and  $h_{13}(l) + e_1^{(3)}(l)$  are separately quantized to symbols in  $\mathcal{A}$ , and are then added before the transmission. Similarly, in Fig. 8, the key-rate of the Algebraic SQGSK protocol is compared with AQGSK-I, wherein the sum  $h_{12}(l) + e_1^{(2)}(l) + h_{13}(l) + e_1^{(3)}(l)$  is directly quantized to  $\mathcal{A}$ . In both AQGSK-I and AQGSK-II, only node-1 quantizes, while the other nodes use their noisy observation of the CSR. When comparing AQGSK-I and Algebraic SQGSK, although points from  $\mathcal{A}$  are transmitted by node-1, the average transmit power in Phase 4 is not the same since the PMF on the points in  $\mathcal{A}$  are different. As a result, the constellations are appropriately scaled so that the average transmit powers in phase 4 are identical. However, when comparing AQGSK-II and SQGSK, no normalization is required as the average transmit powers are identical to start with. As discussed in Section IV-D, in both AQGSK-II and SQGSK, node-1 discards the samples from coherence-blocks wherein the CSR are uniquely decodable by an external eavesdropper.

We evaluate the key-rate of the above protocols for different SNR values (where  $\text{SNR} \triangleq \frac{1}{\sigma^2}$ ) against a given bit-error-rate (BER). A bit is said to be in error if any two nodes disagree with the value at that location. At each SNR value, the threshold values and the excursion length of the level-crossing

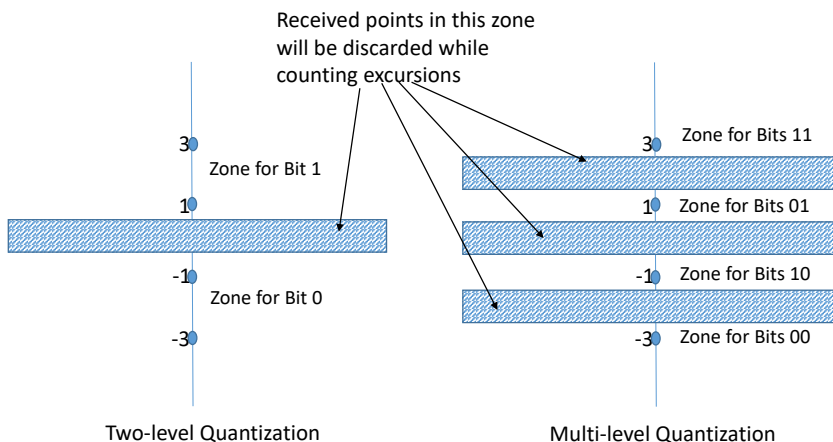


Fig. 9. Depicting the difference between two-level quantization and multi-level quantization while computing excursions at each node. In this example, the in-phase part of the symbols of 16-QAM constellation is used.

algorithm are varied to obtain the same BER for the schemes under comparison. The key-rate of the proposed protocols are presented in Fig. 7 and Fig. 8 for SNR = 10, 20, and 30 dB when used with 4-, 16-, and 64-QAM. The plots in Fig. 7 show that SQGSK outperforms its baseline AQGSK-I. Specifically, the benefits are prominent for 4-QAM; this is because, with just two levels of quantization, cancellation of quantized version of the channel is perfect in most cases during Phase 4. However, as the constellation size increases, different nodes have different quantized versions of the channels due to estimation error, and as a result cancellation at node-2 and node-3 are not perfect. Overall, despite diminishing benefits with larger constellations, SQGSK outperforms AQGSK-II. With reference to the Algebraic SQGSK protocol, Fig. 8 shows that Algebraic SQGSK yields higher key-rate than its baseline AQGSK-I. Specifically, the benefits are prominent at 20 dB and 30 dB; this is because, at high SNR values, recovery of  $\theta(l)$  in Phase 4 is accurate in most cases, and as a result, cancellation of the quantized version of the channel is perfect. However, at lower SNR values, different nodes have different quantized versions, and as a result cancellation at node-2 and node-3 are not perfect. This inference is a generalization of the results observed in Section V-C for  $\sigma^2 = 0$ .

## VII. KEY GENERATION WITH MULTI-LEVEL QUANTIZATION

In this section, we present simulation results on key-rate by using a multi-level quantization algorithm in conjunction with the proposed SQGSK protocols. This approach, in contrast to the two-level algorithm

(applied in the previous section), can generate at most  $\log_2(\sqrt{M})$  bits from a real sample in consensus, where  $M = 2^m$ , for some even  $m$ , denotes the size of  $\mathcal{A}$ . Before presenting the results, we first explain the idea behind multi-level quantization.

### A. Multi-level Quantization

Recall that we have used regular square QAM constellations for  $\mathcal{A}$ , which can be written as  $\mathcal{A} = \mathcal{A}_I \oplus i\mathcal{A}_Q$ , where  $\mathcal{A}_I = \mathcal{A}_Q$ , each of size  $\sqrt{M}$ . Since the in-phase and the quadrature-phase components of  $h_{jk}(l)$  are independently quantized at each node, we only consider the in-phase components for this discussion. Furthermore, we denote the elements of  $\mathcal{A}_I$  by  $a_n$  for  $1 \leq n \leq \sqrt{M}$ , and denote the spacing between successive values by  $\Delta$ , i.e.,  $\min_{n \neq n'} |a_n - a_{n'}| = \Delta$  for  $a_n, a_{n'} \in \mathcal{A}_I$ . Around each value  $a_n \in \mathcal{A}_I$ , we define a zone of width  $\beta(a_n)$  so as to neglect the values lying outside that zone. For illustration purpose, we refer the readers to Fig. 9, which depicts the concept of zones for the in-phase components of 16-QAM, wherein  $\Delta = 2$ . In this example, in order to quantize a real sample to the symbol 1, the sample must lie between  $q$  and  $2 - q$ , for some  $0 < q < 0.5$ . Here, the parameter  $q$  is used to optimize the performance of the proposed algorithm. This implies that the zone size for the points  $\{-1, 1\}$  is  $2 - 2q$ , which is depicted by the white patches in Fig. 9. Note that a real value will be discarded when computing excursions if it lies in one of the blue patches. For the point with maximum value in  $\mathcal{A}_I$ , i.e.,  $a_n = 3$ , the real sample will be quantized to it if it lies anywhere above  $2 + q$ . Similarly, for the other extreme value  $-3$ , the samples that lie anywhere below  $-2 - q$  will be mapped to it. We refer to this form of quantization as multi-level quantization.

### B. Simulation Results

When using multi-level quantization, the nodes are said to be in consensus if the quantized versions of the corresponding samples are in the same zone. In the case of SQGSK, with respect to the CSR  $h_{13}(l)$ , the observation of  $h_{13}(l)$  witnessed at node-2 is unquantized, and therefore, applying multi-level quantization can either result in a discarded sample (by the virtue of the sample lying in a blue patch as per Fig. 9) or a legitimate sample in the white patch of one of the  $\sqrt{M}$  levels. Unlike SQGSK protocol, in the Algebraic SQGSK protocol, the recovery process at node-2 involves a sequence of MAP decoding and successive cancellation, which in turn forces the samples to be in one of the  $\sqrt{M}$  zones. As a result, the zone-concept in multi-level quantization is not directly applicable as the nodes decode the observations to one of the  $\sqrt{M}$  levels. In Fig. 10 and Fig. 11, we present simulation results on the key-rate with multi-level quantization by employing both SQGSK and Algebraic SQGSK protocols, respectively. We have used 16- and 64-QAM at 20 dB and 30 dB to demonstrate the benefits of multi-level



quantization. Using each excursion in consensus, multi-level quantization generates 2- and 3-bits with 16- and 64-QAM, respectively. The bit-mapping from  $\sqrt{M}$  zones to  $\log_2(\sqrt{M})$  bits is chosen such that ones and zeros in the generated secret-key are equiprobable. The plots show that at 20 dB SNR, multi-level quantization algorithm performs poorly when using 64-QAM; this is because the effective noise (a combination of the recovery noise and channel estimation noise) at the nodes results in quantizing their samples to different levels, thereby resulting in errors<sup>3</sup>. However, at 30 dB, the plots show that multi-level quantization provides benefits, and this behavior follows our intuition that low variance of noise rarely takes the samples outside quantization zones.

In summary, stitching together the advantages of two-level and multi-level quantization, we recommend Algebraic SQGSK protocol along with the two-level crossing algorithm at low and moderate SNR values, whereas we recommend Algebraic SQGSK protocol along with the multi-level quantization algorithm at high SNR values. Finally, between SQGSK and Algebraic SQGSK, we recommend the latter scheme due to zero leakage of the CSR to an external eavesdropper.

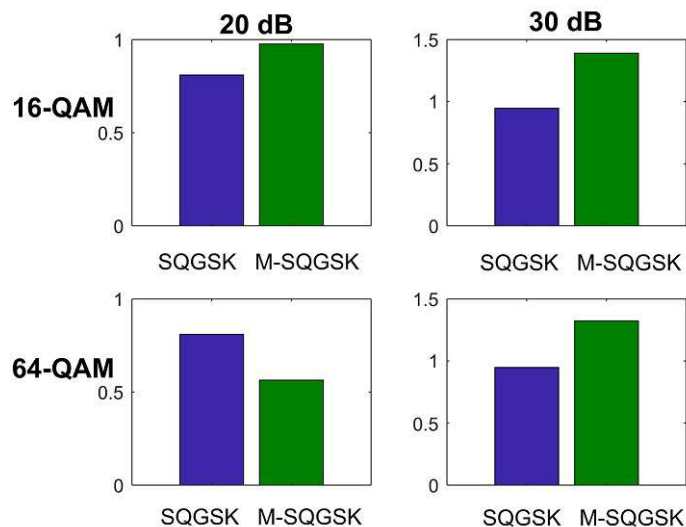


Fig. 10. Key-rate using the SQGSK protocol with and without multi-level quantization algorithm. In the above figure, SQGSK and M-SQGSK refer to two-level SQGSK and multi-level SQGSK, respectively. To generate the above results, BER was held at 5% and 1% at 20 dB and 30 dB, respectively.

## VIII. DISCUSSION

We address physical-layer GSK generation in a wireless network wherein the nodes have the constraint of transmitting baseband symbols from finite complex constellations. We proposed practical GSK proto-

<sup>3</sup>We have observed that multi-level quantization performs poorer than two-level quantization at 10 dB SNR too, and hence we have omitted those results

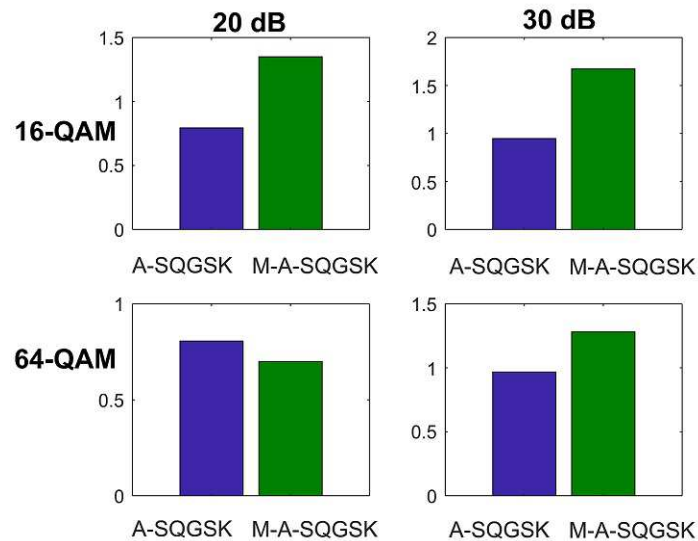


Fig. 11. Key-rate using the Algebraic SQGSK protocol with and without multi-level quantization algorithm. In the above figure, A-SQGSK and M-A-SQGSK refer to two-level Algebraic SQGSK and multi-level Algebraic SQGSK, respectively. To generate the above results, BER was held at 2% and 1% at 20 dB and 30 dB, respectively.

cols in a three-node wireless network, wherein in addition to the facilitator, the other nodes in the network also quantize their channel estimates and then use them appropriately to improve the correlation among the CSR. We first proposed the Symmetrically Quantized GSK protocol (SQGSK), which provided higher key-rate in comparison with the traditional baselines. However, we also noticed that the leakage of the CSR with SQGSK is significant. In order to circumvent the leakage issues in SQGSK, we proposed the Algebraic SQGSK protocol, which guarantees zero-leakage to the eavesdropper and yet outperforms the traditional AGSK-I protocol. We have provided extensive simulation results to showcase the benefits of the proposed protocols. As a future direction of research, we intend to develop practical key generation protocols for a wireless network with more than three nodes, and with varying topology.

#### ACKNOWLEDGEMENTS

This work was supported by the New Faculty Seed Grant - PLN06R to J. Harshan from the Indian Institute of Technology Delhi.

#### REFERENCES

- [1] Suhas Mathur , Narayan M , Chunxuan Ye , Alex Reznik, "Radio-telepathy: extracting a secret key from an unauthenticated wireless channel," *Mobicom 2008*.
- [2] C. Ye, S. Mathur, A. Reznik, Y. Shah, W. Trappe and N. B. Mandayam, "Information-theoretically secret key generation for fading wireless channels," in *IEEE Trans. on Information Forensics and Security*, vol. 5, no. 2, pp. 240-254, June 2010.
- [3] A. J. Pierrot, R. A. Chou, M. R. Bloch, "The effect of eavesdroppers statistics in experimental wireless secret key generation", submitted to *IEEE Trans. on Information Forensics and Security*. Available online at arXiv:1312.3304 [cs.IT], June 2014.

- [4] S. Gollakota and D. Katabi, "Physical layer wireless security made fast and channel independent," *IEEE INFOCOM, 2011*, Shanghai, 2011, pp. 1125-1133.
- [5] Y. Liu, S. C. Draper and A. M. Sayeed, "Exploiting channel diversity in secret key generation from multipath fading randomness," in *IEEE Trans. on Information Forensics and Security*, vol. 7, no. 5, pp. 1484-1497, Oct. 2012.
- [6] K. Ren, H. Su and Q. Wang, "Secret key generation exploiting channel characteristics in wireless communications," in *IEEE Trans. on Wireless Communications*, vol. 18, no. 4, pp. 6-12, Aug. 2011.
- [7] T. H. Chou, A. M. Sayeed and S. C. Draper, "Minimum energy per bit for secret key acquisition over multipath wireless channels," *IEEE ISIT 2009*, Seoul, 2009, pp. 2296-2300.
- [8] C. Ling, L. Luzzi and M. R. Bloch, "Secret key generation from Gaussian sources using lattice hashing," *IEEE ISIT 2013*, Istanbul, 2013, pp. 2621-2625.
- [9] Yanpei Liu, S. C. Draper and A. M. Sayeed, "Secret key generation through OFDM multipath channel," *45th Annual Conference on Information Sciences and Systems 2011*, Baltimore, MD, 2011, pp. 1-6.
- [10] K. Zeng, D. Wu, A. Chan and P. Mohapatra, "Exploiting multiple-antenna diversity for shared secret key generation in wireless networks," *IEEE INFOCOM, 2010*, San Diego, CA, 2010, pp. 1-9.
- [11] K. Kravtsov, Z. Wang, W. Trappe, and P. Prucnal, "Physical layer secret key generation for fiber-optical networks," *Opt. Express*, 21, pp. 23756-23771, 2013.
- [12] L. Lai, Y. Liang and H. V. Poor, "A unified framework for key agreement over wireless fading channels," in *IEEE TIFS*, vol. 7, no. 2, pp. 480-490, April 2012.
- [13] H. Zhou, L. M. Huie and L. Lai, "Secret key generation in the two-way relay channel with active attackers," in *IEEE Trans. on Information Forensics and Security*, vol. 9, no. 3, pp. 476-488, March 2014.
- [14] T. Shimizu, H. Iwai and H. Sasaoka, "Physical-layer secret key agreement in two-way wireless relaying systems," in *IEEE Trans. on Information Forensics and Security*, vol. 6, no. 3, pp. 650-660, Sept. 2011.
- [15] C. D. T. Thai, J. Lee and T. Q. S. Quek, "Physical-layer secret key generation with colluding untrusted relays," in *IEEE Trans. on Wireless Communications*, vol. 15, no. 2, pp. 1517-1530, Feb. 2016.
- [16] R. Zhang, L. Song, Z. Han and B. Jiao, "Physical layer security for two-way untrusted relaying with friendly jammers," in *IEEE Trans. on Vehicular Technology*, vol. 61, no. 8, pp. 3693-3704, Oct. 2012.
- [17] X. He and A. Yener, "Two-hop secure communication using an untrusted relay", *EURASIP Journal on Wireless Communications and Networking*, 2009.
- [18] C. Ye and A. Reznik, "Group secret key generation algorithms," *IEEE ISIT 2007*, Nice, France, 2007, pp. 2596-2600.
- [19] Y. Wei, C. Zhu and J. Ni, "Group secret key generation algorithm from wireless signal strength," *Sixth International Conference on Internet Computing for Science and Engineering 2012*, Henan, 2012, pp. 239-245.
- [20] P. Xu, K. Cumanan, Z. Ding, X. Dai and K. K. Leung, "Group secret key generation in wireless networks: algorithms and rate optimization," in *IEEE Trans. on Information Forensics and Security*, vol. 11, no. 8, pp. 1831-1846, Aug. 2016.
- [21] H. Liu, J. Yang, Y. Wang, Y. J. Chen and C. E. Koksal, "Group secret key generation via received signal strength: protocols, achievable rates, and implementation," in *IEEE Trans. on Mobile Computing*, vol. 13, no. 12, pp. 2820-2835, Dec. 2014.
- [22] C. D. T. Thai, J. Lee and T. Q. S. Quek, "Secret group key generation in physical layer for mesh topology," *IEEE GLOBECOM 2015*, San Diego, CA, 2015, pp. 1-6.
- [23] J. Harshan, Sang-Yoon Chang, and Yih-Chun Hu, "Insider-attacks on physical-layer group secret-key generation in wireless networks," in the Proc. of *IEEE WCNC 2017*, San Francisco, USA, March 2017.
- [24] J. Harshan and B. S. Rajan, "On two-user Gaussian multiple access channels with finite input constellations," in *IEEE Trans. on Information Theory*, vol. 57, no. 3, pp. 1299-1327, March 2011.
- [25] Manish Rao and J. Harshan, "Practical Physical-Layer Group Secret-Key Generation in Three-User Wireless Networks," in the Proc. of *International Conference on Signal Processing and Communications*, 2018.